

3D self-organized microvascular model of the human blood-brain barrier with endothelial cells, pericytes and astrocytes

Original

3D self-organized microvascular model of the human blood-brain barrier with endothelial cells, pericytes and astrocytes / Campisi, Marco; Shin, Yoojin; Osaki, Tatsuya; Hajal, Cynthia; Chiono, Valeria; Kamm, Roger D.. - In: BIOMATERIALS. - ISSN 0142-9612. - ELETTRONICO. - 180:(2018), pp. 117-129. [10.1016/j.biomaterials.2018.07.014]

Availability:

This version is available at: 11583/2716982 since: 2018-11-10T16:56:49Z

Publisher:

Elsevier Ltd

Published

DOI:10.1016/j.biomaterials.2018.07.014

Terms of use:

This article is made available under terms and conditions as specified in the corresponding bibliographic description in the repository

Publisher copyright

Elsevier postprint/Author's Accepted Manuscript

© 2018. This manuscript version is made available under the CC-BY-NC-ND 4.0 license
<http://creativecommons.org/licenses/by-nc-nd/4.0/>. The final authenticated version is available online at:
<http://dx.doi.org/10.1016/j.biomaterials.2018.07.014>

(Article begins on next page)

3D Self-Organized Microvascular Model of the Human Blood-Brain Barrier with Endothelial Cells, Pericytes and Astrocytes

Marco Campisi^{1,2}, Yoojin Shin², Tatsuya Osaki², Cynthia Hajal², Valeria Chiono¹, Roger D. Kamm^{2,3,4 *}

¹ Department of Mechanical and Aerospace Engineering, Politecnico di Torino, Corso Duca degli Abruzzi 24, 10129 Turin, Italy.

² Department of Mechanical Engineering, Massachusetts Institute of Technology, 500 Technology Square, MIT Building, Room NE47-321, Cambridge, MA, 02139, United States of America.

³ Department of Biological Engineering, Massachusetts Institute of Technology, 500 Technology Square, MIT Building, Room NE47-321, Cambridge, MA, 02139, United States of America.

⁴ Singapore-MIT Alliance for Research&Technology (SMART), BioSystems and Micromechanics (BioSym), Singapore, Singapore.

*Corresponding author: Roger D. Kamm: rdkamm@mit.edu

Keywords: Human Blood-Brain Barrier; *In Vitro* Modeling; Microfluidic Device; Self-Assembled Microvascular Network; Induced Pluripotent Stem Cell-Derived Endothelial Cells; Drug Delivery Test Platform.

Abstract

The blood-brain barrier (BBB) regulates molecular trafficking, protects against pathogens, and prevents efficient drug delivery to the brain. Models to date failed to reproduce the human anatomical complexity of brain barriers, contributing to misleading results in clinical trials. To overcome these limitations, a novel 3-dimensional BBB microvascular network model was developed via vasculogenesis to accurately replicate the *in vivo* neurovascular organization. This microfluidic system includes human induced pluripotent stem cell-derived endothelial cells, brain pericytes, and astrocytes as self-assembled vascular networks in fibrin gel. Gene expression of membrane transporters, tight junction and extracellular matrix proteins, was consistent with computational analysis of geometrical structures and quantitative immunocytochemistry, indicating BBB maturation and microenvironment remodeling. Confocal microscopy validated microvessel-pericyte/astrocyte dynamic contact-interactions. The BBB model exhibited perfusable and selective microvasculature,

34 with permeability lower than conventional *in vitro* models, and similar to *in vivo* measurements in rat
35 brain. This robust and physiologically relevant BBB microvascular model offers an innovative and
36 valuable platform for drug discovery to predict neuro-therapeutic transport efficacy in pre-clinical
37 applications as well as recapitulate patient-specific and pathological neurovascular functions in
38 neurodegenerative disease.

39

40 Introduction

41

42 The blood-brain barrier (BBB) and blood-spinal cord barrier help maintain brain homeostasis [1] by
43 regulating the transport of necessary nutrients, ions, and hormones, while preventing the entry of
44 neurotoxins or pathogens into the brain owing to a complex membrane transport mechanism [2]. The
45 BBB consists of specialized endothelial cells (ECs) interconnected by junctional complexes including
46 tight junctions (TJs) and adherens junctions, surrounded by pericytes (PCs) and astrocytes (ACs), and
47 ensheathed in a basal lamina. Each of these specialized features contributes to BBB integrity, and to
48 the control of transport processes [3]. Loss of BBB integrity is associated with Alzheimer's disease
49 [4][5], Parkinson's disease [6], and multiple sclerosis [7], as well as with brain cancer [8].
50 Furthermore, the BBB regulates active and passive transport of solutes into the brain [9][10], posing
51 an obstacle to drug delivery for the treatment of neurological diseases and brain tumors [11][12].

52

53 For these reasons, preclinical models of the BBB are developed to understand its role in the
54 pathogenesis of neurological diseases as well as to evaluate drug permeability. For years, *in vivo*
55 animal models have been used to model the BBB and study drug delivery [13]. Although these
56 techniques are considered the gold standard, 80% of successful drug candidates in animal models
57 later failed in clinical trials [14][15].

58

59 To optimize the design of innovative therapies and drug carriers, a robust, reliable, and cost-effective
60 *in vitro* BBB model that adequately reflects human *in vivo* conditions is required [16][17]. For several
61 decades, transwell assays have been widely adopted to assess drug permeability by culturing a
62 confluent monolayer of ECs in the absence or presence of PCs or ACs [18]. Although this system is
63 reproducible and easy to use, it has limitations in mimicking fundamental BBB features and
64 microenvironmental complexities such as cell-cell or cell-matrix interactions, compromising its
65 ability to accurately model brain capillaries in terms of junctional proteins and membrane transporter

66 expression [17][19][20]. Recently, BBB spheroids have been developed to study organogenesis and
67 the transport of brain penetrating agents [21][22]. Although these systems are cost-effective, they are
68 limited in their ability to recreate a realistic and relevant BBB morphology. As an alternative to
69 simple culture models, microfluidic technology offers a promising tool for reconstituting the BBB
70 with several advantages: microfluidic systems allow for precise control of the 3D cellular and
71 extracellular matrix (ECM) microenvironment, while providing a platform for the study of cellular
72 and structural responses to various stimuli. These systems mimic the complex cellular interactions
73 and structures found in many tissues or organs *in vivo*, and are thus referred to as 'organ-on-a-chip'
74 [23][24]. Recently, efforts to reconstitute a 3D BBB model within a microfluidic system have
75 accelerated with the development of organ-on-a-chip assays to study immune cell transmigration [25],
76 metastatic cancer extravasation to the brain [26], as well as vessel formation in a tubular shape [27].
77 However, systems to date have relatively large diameters (~ 600-800 μm) [27] compared to the
78 dimension of human BBB vasculature *in vivo* (arterioles and venules 10-100 μm ; capillaries 7-10
79 μm) [28][29], and fail to recapitulate BBB microvasculature morphology and development in terms
80 of mature cell-cell interactions via natural biological processes, as well as physiological blood flow
81 rates and wall shear stresses needed to activate mechanosensing/mechanotransduction pathways, thus
82 altering realistic transport exchange mechanisms at the level of brain capillaries [30][31].

83
84 Two microfluidic models have been recently reported using a co-culture of human ECs and rat
85 neurons and ACs. One incorporated a compartmentalized 3D monolayer of human cerebral
86 microvascular ECs in co-culture with primary rat ACs and neurons [32]. In a separate study, similar
87 to the previous model [33], a BBB microvascular network (μVN) platform created by a
88 vasculogenesis-like process, culturing human umbilical vein endothelial cells (HUVECs) in a 3D
89 ECM-mimetic hydrogel showed that direct interaction with neural tissue from the rat cortex was
90 responsible for the low permeability values measured [34].

91

92 However, while co-cultures with cells from different species are advantageous in terms of
93 accessibility and ease of genetic manipulations, cross-species compatibility remains a concern
94 regarding the relevance of these results to human physiology [35]. Moreover, HUVECs offer a poor
95 model for cerebral vasculature, while PCs, recognized to be a key component of the BBB [35], have
96 not been considered in these models [32][34].

97

98 To address the main limitations of the current state-of-the-art models, we reasoned that a BBB model
99 developed from human cells co-cultured in a 3D microenvironment would better replicate the human
100 BBB, based on the hypothesis that the co-culture arrangement could support the maturation and
101 differentiation of human iPSC cell-derived endothelial cells (iPSC-ECs) into BBB microvascular cells.
102 Hence, a 3D BBB microfluidic model was designed consisting of self-assembled μ VNs from human
103 iPSC-ECs as well as human primary brain PCs, and human primary ACs, where all cell types
104 spontaneously assembled into a modular organization reproducing the BBB structure being in
105 dynamic and direct contact with each other.

106

107 BBB functionality was evaluated by progressive increase of co-culture complexity up to a tri-culture
108 of iPSC-ECs, PCs, and ACs. Confocal imaging and immunocytochemistry, permeability
109 measurements and gene expression analysis were used to quantitatively assess BBB characteristics.
110 Such human 3D BBB model has unique biological features, representing a promising platform for *in*
111 *vitro* preclinical experimentation.

112

113 **Materials and methods**

114

115 **Fabrication of the microfluidic device (micro-device/macro-device)**

116 The 3D microfluidic systems were composed of polydimethylsiloxane (PDMS; Sylgard 184; Dow
117 Corning, MI, USA) with a single layer microchannel and two fluid channels, fabricated by soft
118 lithography [36] (Fig. 1c, Supplementary Fig. 1a-b). Elastomer and curing agent were mixed (10:1
119 volume ratio), degassed and poured onto a silicon master and cured overnight at 60°C. I/O holes were
120 created with biopsy punches, then the device was taped to remove dust and sterilized as previously
121 described [37]. The PDMS micro and macro-devices were treated with oxygen plasma (Harrick
122 Plasma), then bonded to a glass coverslip (Fisher Scientific) coated with poly(D-lysine
123 hydrobromide) (PDL, Sigma-Aldrich) solution (1 mg/ml) and, finally, placed in an incubator for 3 h
124 at 37°C, rinsed 3 times and dried overnight.

125

126 **Cell culture and device seeding of BBB self-assembled vascular network model**

127 Human iPSC-ECs (Cellular Dynamics International, CDI) were subcultured on flasks coated with
128 human fibronectin (30 µg/ml, Millipore) in vascular medium (VasculLife VEGF Medium Complete
129 Kit, icell media supplement, CDI). Pericytes and astrocytes isolated from human brain (ScienCell),
130 were cultured in growth medium (ScienCell) on a poly-L-lysine (Sigma-Aldrich) coated flask, and
131 maintained in a humidified incubator (37 °C, 5% CO₂), replacing the medium every 2 days. Cells
132 were detached using TrypLE (for iPSC-ECs) and 0.025% trypsin/EDTA for other cell types (Thermo
133 Fisher). Experiments were performed between passages 3 and 5 for all cells.

134

135 Fibrinogen (6 mg/ml) and thrombin (100 U/ml) from bovine plasma (Sigma-Aldrich) were separately
136 dissolved in sterile PBS. Then, thrombin was mixed with 1ml of EGM-2 MV (Lonza) and placed on
137 ice. Cells were detached and spun down at 1200 rpm for 5 min and cell pellet was resuspended in
138 EGM-2 MV 4 U/ml thrombin. Cell suspension was mixed with fibrinogen (final concentration 3

139 mg/ml) at 1:1 volume ratio. The mixture was quickly pipetted into the gel filling ports. Devices were
140 placed in a humidified enclosure and allowed to polymerize at room temperature (RT) for 15 min
141 before the fresh medium was introduced to fluidic channels. iPSC-ECs medium was supplemented
142 with 50 ng/ml of vascular endothelial growth factor (VEGF, Peprotech), for the first four days of
143 culture. Medium for the tri-culture condition was supplemented with 1% (vol/vol) Astrocyte Growth
144 factor (AGF, astrocyte growth supplement, ScienCell).

145
146 Three different cell combinations were tested: 1) iPSC-ECs mono-culture (6×10^6 cells/ml), 2) co-
147 culture iPSC-ECs+PCs (add 2×10^6 cells/ml PCs) and 3) tri-culture of iPSC-ECs+PCs+ACs (add
148 2×10^6 cells/ml ACs). After fibrin polymerization, medium channels were coated for 30 min in an
149 incubator (37°C 5% CO₂) with human fibronectin (60 µg/ml) to promote endothelial cell adhesion.
150 In each case, iPSC-ECs were subsequently seeded at 2×10^6 cells/ml in EBM-2 (Lonza) into the fluidic
151 channels to reduce diffusion of fluorescent dyes into the gel. Non-adherent cells were removed after
152 2 h. The device was kept in an incubator for 7 days (37 °C, 5% CO₂), 200 µl of medium was replaced
153 every 24 h. Devices prepared in this manner were used for both permeability measurements and
154 immunocytochemical staining. PC conditioned medium was collected after 3 days, from a T75 flask
155 of PCs culture, mixed 1:1 volume ratio with fresh medium and replaced every 24 h in the iPSC-ECs
156 mono-culture in the microfluidic device.

157
158 The *in vitro* BBB model was developed by co-culturing human iPSC-ECs, and human brain PCs and
159 ACs to mimic certain aspects of the organization and structure of the brain microcirculation observed
160 *in vivo* (Fig. 1a,b). The BBB model formed by a vasculogenesis-like process, consisted of a well-
161 connected and perfusable µVN in a microfluidic device (Fig. 1c, Supplementary Fig. 1a), interacting
162 via paracrine, juxtacrine and mechanical signaling[38][39]. iPSC-ECs seeded in the side media
163 channels reduced leakage through the side walls of the central gel region and promoted the formation
164 of patent vessel connections to the media channels, facilitating flow into the network (Fig. 1d,e).

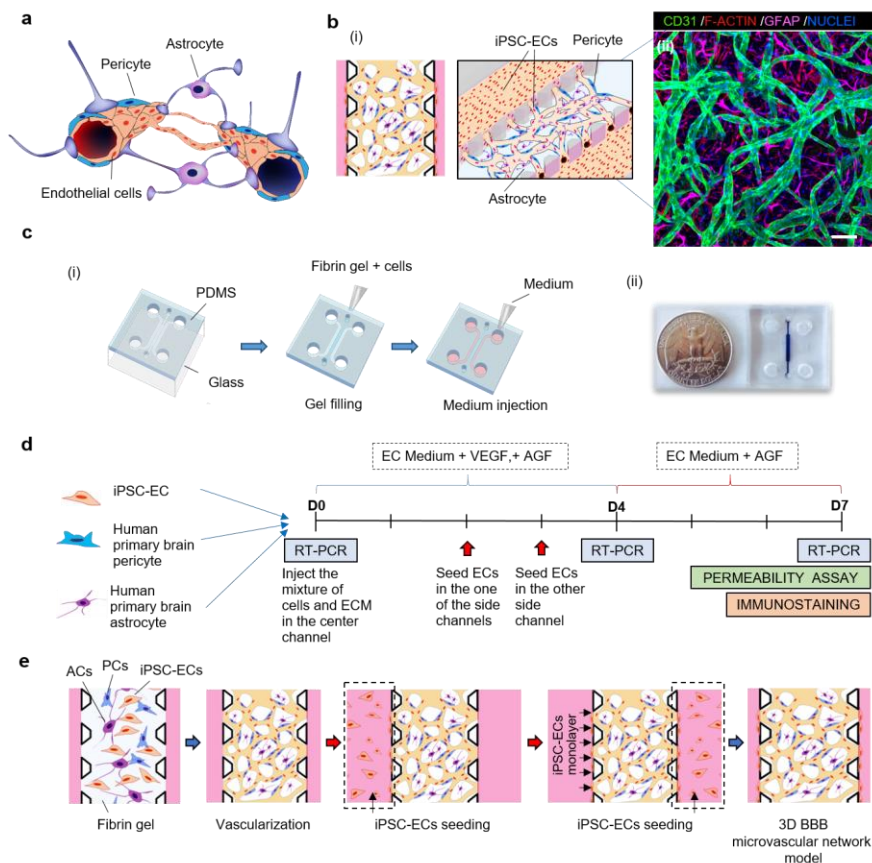


Figure 1: Blood-brain barrier and *in vitro* microvascular network model. (a) Schematic representation of the blood-brain barrier (BBB), composed of brain Endothelial cells (ECs) vessels overlapped by pericytes (PCs) and astrocytes (ACs) endfeet. (b, i) Schematic representation of proposed 3D BBB microvascular network (μ VN) model that mimics the microvascular structure present in the brain environment. (b, ii) Confocal image of self-assembled BBB μ VN model including iPSC-ECs (CD31, green), PCs (F-actin, red) and ACs (GFAP, magenta), and nuclei (DAPI, blue). (c) Microfluidic device fabrication: (c, i) PDMS mold with patterned channels were produced by soft lithography and bonded to a glass coverslip. The central gel region contained cells and hydrogels, side channels and reservoirs were filled with cell culture medium. (c, ii) A photo of the microfluidic device. (d) Timeline of the experiments. (e) Cell seeding configuration and experimental steps of vasculogenesis process of BBB μ VN model including iPSC-ECs+PCs+ACs as self-assembled microvascular network and 3-dimensional ECs layer covering top, bottom and side surfaces of the fluidic channel. Scale bar (b, ii) indicates 100 μ m.

180 Immunocytochemistry and confocal imaging

181 The 3D BBB μ VNs were cultured for 7 days followed by rinsing in PBS and fixation in 4%
182 paraformaldehyde (PFA, Electron Microscopy Sciences) for 15 min at RT. Cell membranes were
183 permeabilized with 0.1% Triton X-100 (Sigma-Aldrich) for 5 min at RT and washed twice with PBS.
184 Primary antibodies (1:100, volume ratio) against CD31, Glial Fibrillary Acidic Protein (GFAP),
185 (Abcam), F-actin (Rhodamine Phalloidin, Molecular Probes), 4',6-Diamidino-2-Phenylindole (DAPI
186 Thermo Fisher Scientific), were used to identify, respectively, iPSC-ECs, ACs, PCs, and nuclei.

187 F-actin is strongly expressed in all cells present in our model, whereas only iPSC-ECs highly express
188 CD31 and only astrocytes express GFAP. We therefore used double staining of CD31/F-actin to
189 identify iPSC-ECs and GFAP/F-actin to identify ACs, which enabled us to clearly identify the PC
190 population as those cells that only express F-actin.

191 To characterize the presence of TJs and ECM proteins by immunocytochemistry, primary antibodies
192 were used against: ZO-1 (Invitrogen), occludin, claudin-5, laminin and collagen IV (Abcam).
193 Secondary antibodies (1:200, volume ratio) were anti-rabbit or anti-mouse IgG conjugated with Alexa
194 Fluor (488-555, or 647) (Invitrogen). Detail on primary and secondary antibodies are listed in
195 Supplementary Table 2. Devices were incubated with primary and secondary antibodies overnight at
196 4°C, placed on a shaker. After PBS washing, devices were imaged using a confocal laser scanning
197 microscope (FMV-1000, Olympus, Japan) (aspect ratio 1024×1024) high resolution images at
198 1000/pixel scan velocity. Phase contrast imaging was used for morphological observations at different
199 culture time-points (Axiovert 200, Zeiss, Germany). Post-processing and stitching for tiled images
200 were performed using Imaris (Bitplane, Switzerland) and Fluoview (Olympus, Japan). Fold change
201 average immunofluorescent (IF) intensity (relative to iPSC-ECs) was calculated by dividing total
202 immunofluorescent intensity by cell boundary length (ZO-1, occludin, and claudin-5) or by
203 vascularized area (laminin, collagen IV). ROIs were selected to contain only microvascular portions
204 such that no part outside the vessels were included in the computations.

205

206 **Characterization of BBB microvascular parameters**

207 To characterize microvascular parameters, confocal images were analyzed using ImageJ software
208 (<http://rsbweb.nih.gov/ij/>) and plugins (Trainable Weka Segmentation 3D, 3D geometrical measure).
209 Briefly, raw images were prepared by enhancing contrast and removing noise. An automatic threshold
210 was used to produce binarized images. From 2D projections, lateral vessel area ($A_{lateral}$), and total
211 branch length (L_{branch}) were computed by ImageJ. Percentage of area coverage was calculated
212 dividing $A_{lateral}$ by the entire area of the region of interest. Taking advantage of the observation that
213 most vessels are oriented in a plane parallel to the glass substrate, lateral diameters, parallel to the
214 glass substrates of the devices, were computed as the ratio of the projected lateral vessel area to the
215 total branch length. Transverse diameters, perpendicular to the glass substrate, were computed using
216 the 3D vessel volume (V) and the surface area of the vessels in 3D ($A_{surface}$). Average cross-section
217 area and circularity were computed using lateral and transverse diameters. The sequences of
218 instructions and equations used to compute both diameters, cross-section, lateral and surface areas
219 and circularity are shown in Supplementary methods.

220

221 **Microvascular network perfusion and fluorescent dextran-based permeability assay**

222 To assess permeability of the 3D BBB model, solutions containing 10 or 40 kDa FITC-dextran
223 (Sigma-Aldrich) were introduced as fluorescent tracers, and time-sequential images to assess leakage
224 through the microvascular barrier were captured. Briefly, after 7 days of culture, each device was
225 moved to the confocal conditioning chamber (37°C, 5% CO₂), culture medium was aspirated from
226 all reservoirs in each side channel. Then, 5 µl of dextran solution in PBS was injected in one side,
227 simultaneously with 5 µl of medium on the other fluidic channel to maintain equal hydrostatic
228 pressures in the device. Confocal images were acquired every 3-5 min for 6 to 8 times to create the

entire 3D stack of the gel volume with microvascular formation at each time point. ROIs were selected considering vascular networks with a clear boundary between vessel wall and gel regions.

231

To assess perfusability, fluorescent tracers (FITC-dextran) were introduced through the microvascular networks by imposing a hydrostatic pressure drop across the gel region between two medium channels. Videos were recorded using NIS-Elements software (NIKON) on a fluorescent microscope (Nikon, TI-E ECLIPSE.) at 30 frames per second.

236

237 **Quantification of vessel permeability coefficient**

The vascular permeability is evaluated as the flux of solute across the walls of the vascular network. Using mass conservation, the quantity of FITC-dextran crossing the vascular network equals the rate at which it accumulates outside the vessels in the tissue gel region. According to a previously described method[40], vascular network permeability, P_v , was quantified by obtaining the average intensity of vessels I_v and tissue (outside vessels) I_T at two different time points $t1$ and $t2$ and using:

$$P_v = \frac{1}{(I_v^{t1} - I_T^{t1})} \frac{(I_T^{t2} - I_T^{t1})}{\Delta t} \frac{V}{A_{surface}}$$

244

Here, Δt is the time between two images, V is the tissue volume, $A_{surface}$ is the surface area of all vessels in the selected ROI, computed based on the assumption that the ratio $V/A_{surface}$ can be estimated as the tissue area $A_{lateral}$ divided by the perimeter of the vascular region L_{branch} in the projected 2D images from the 3D confocal stacks. Diffusion of fluorescent dextran into the gel was minimized by introducing an iPSC-ECs monolayer in both side channels. The fluorescence intensity values, vessel surface area and tissue/gel region area were computed using ImageJ.

251

252 **RNA isolation and quantitative RT-PCR**

253 Total RNA was isolated from different conditions using TRIzol reagent (Life Science) for dissolving
254 fibrin gel. Reverse transcription was performed using SuperScript VILO cDNA synthesis kit
255 (Invitrogen). Quantitative Real-time RT-PCR (RT-PCR) using SYBR Premix Ex Taq (Takara) or
256 Power SYBR Green PCR Master Mix, was performed with a 7900HT Fast Real-Time PCR System
257 (Applied Biosystems). mRNA of endothelial cell adhesion molecule (PECAM-1) also known CD31,
258 glyceraldehyde 3-phosphate dehydrogenase (GAPDH) and Ribosomal Protein S18 (RPS18) were
259 used as housekeeping genes, set to 100% as the internal standard. RT-PCR experiments were repeated
260 at least 3 times for cDNA prepared from 6 devices. Primer sequences (Integrated DNA technology)
261 are listed in supplementary Table 1. RT-PCR was performed in a scaled up version a of the device
262 (Supplementary Fig. 1b) in order to collect higher amount of total RNA.

263

264 **Statistical analysis**

265 All data are plotted as mean \pm SD. One-way ANOVA with pairwise comparisons by the Tukey post
266 hoc test was used to determine whether three or more data-sets were statistically significant. Statistical
267 tests were performed using JMP pro (SAS Institutes, Inc.). At least four devices (≥ 2 regions per
268 device) for each condition within 3 independent experiments were used for the imaging and data
269 analysis. **** denotes $p < 0.0001$, *** denotes $p < 0.001$, ** denotes $p < 0.01$, * denotes $p < 0.05$.
270 Non-paired student's t-test was used for significance testing between two conditions.

271

272 Results

273

274 Optimization of self-assembled microvasculature

275 Three models were established, as described in Methods, with progressively greater complexity: (i)
276 iPSC-ECs (Fig. 2a,b (i)), (ii) iPSC-ECs + PCs (Fig. 2a,b (ii)), and (iii) iPSC-ECs + PCs + ACs (Fig.
277 2a,b (iii), Supplementary Figs. 4a-c). In each case, the iPSC-ECs elongated and intracellular
278 intussusception and vacuoles appeared after 1 day followed by the formation of lumen structures after
279 2-3 days (Supplementary Figs. 2a and 3a,b). Further development of the μ VNs resulted in a highly
280 interconnected microvasculature by day 7 of the culture (Fig. 2b).

281

282 With iPSC-ECs alone (Fig. 2a,b (i)), vascular networks formed in 4-5 days (Supplementary Fig. 2a),
283 however, the vessels fused, forming large, elliptical cross-section lumens, many of which contacted
284 the bottom coverslip (Fig. 3a) and gradually degraded and regressed after 7 days (Supplementary Fig.
285 5a). In contrast, co-culture of iPSC-ECs with PCs formed smaller and more highly branched vessels
286 (Figs. 2a,b (ii), 3b). No significant difference could be observed when iPSC-ECs were cultured alone
287 or with PC conditioned medium (Supplementary Fig. 5b), suggesting that contact with PCs effectively
288 facilitated endothelial organization, by stabilizing a mature vasculature with a morphology more
289 similar to that found *in vivo*.

290

291 The addition of ACs further assisted in the development of a complex inter-connected and branched
292 architecture found in native vasculatures (Fig. 2a,b (iii), Supplementary Fig. 3a,b). In tri-culture with
293 ACs, the μ VNs exhibited distinctive behavior during formation, with increased tortuosity and vessels
294 extending higher up in the 3D gel (Fig. 3c). A fundamental characteristic of the BBB is the stratified
295 organization of cells around the vessels and their direct contact interactions. In 4 replicates with 10-
296 12 high resolution confocal images, we observed a spontaneous self-organization into multicellular
297 BBB structures. Indeed, PCs (F-actin, red, Fig. 2c) adhered to both sides of the endothelial cell

Commentato [CM1]: If reviewer would like to specify how many biological replicates/highly resolution confocal, numbers are more than 4 replicates with 10-12 images.

298 surface, surrounding the vessel (CD31, green, Fig. 2c,e, Supplementary Fig. 6a, Supplementary video
299 1). For example, tracing the intensity profiles of EC and PC fluorescence (Fig. 2d), F-actin expression
300 was observed outside the vessel, clearly delineating the presence of PCs. These results showed that
301 pericytes partially overlapped the outer surface of the EC layer exhibiting a BBB-like organization.
302 In addition, 3D rendering of vessel bifurcations showed PCs in contact with the endothelium at
303 multiple locations (Fig. 2e). Moreover, direct physical contacts were observed between AC endfeet
304 (Glial Fibrillary Acidic Protein, (GFAP), violet) and the abluminal surface of the brain vessels (CD31,
305 green, Fig. 2f; Supplementary Figs. 6b,c).

306

307 **Characterization of microvascular parameters**

308 To determine the geometrical changes in the μ VNs (Fig. 3a-c, Supplementary Fig.4a-c), lateral and
309 transverse vessel diameter distributions, percentage of image area containing vascular networks, and
310 total branch length were each quantified (Fig. 3d-i). As expected, in the iPSC-ECs+PCs co-culture,
311 the lateral vessel diameters (30 to 100 μ m, Fig. 3e (i)) were significantly lower than in mono-culture
312 conditions (50 to 150 μ m with a few outliers to 200 μ m, Fig. 3d (i)). Lateral diameters were further
313 reduced by adding ACs (most values between 25 and 50 μ m (Fig. 3f (i))). The overall transverse
314 diameter distributions were similar for all three conditions, ranging between 10 and 40 μ m, and
315 centered around 30 μ m (Fig. 3d-f (ii)).

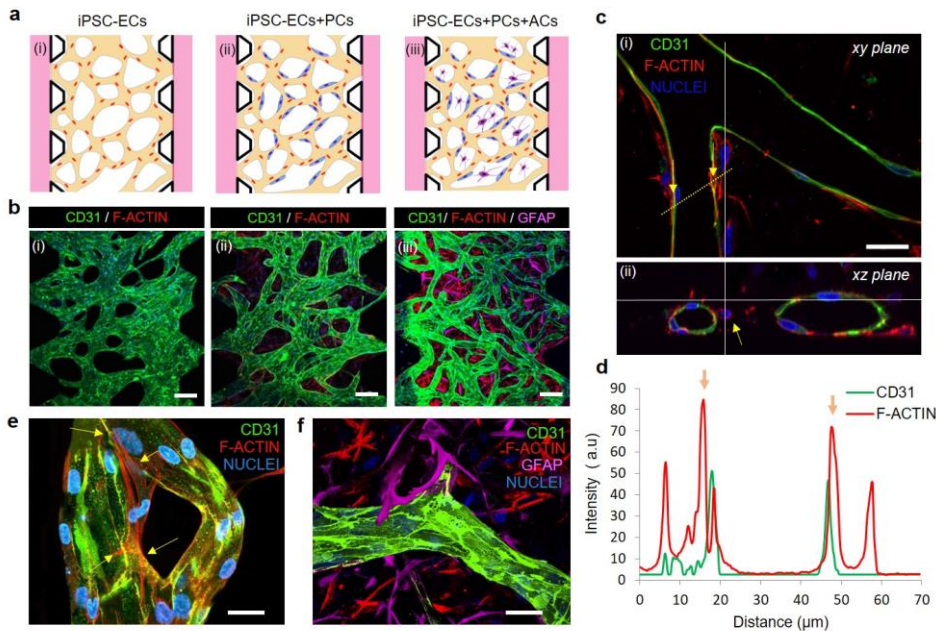
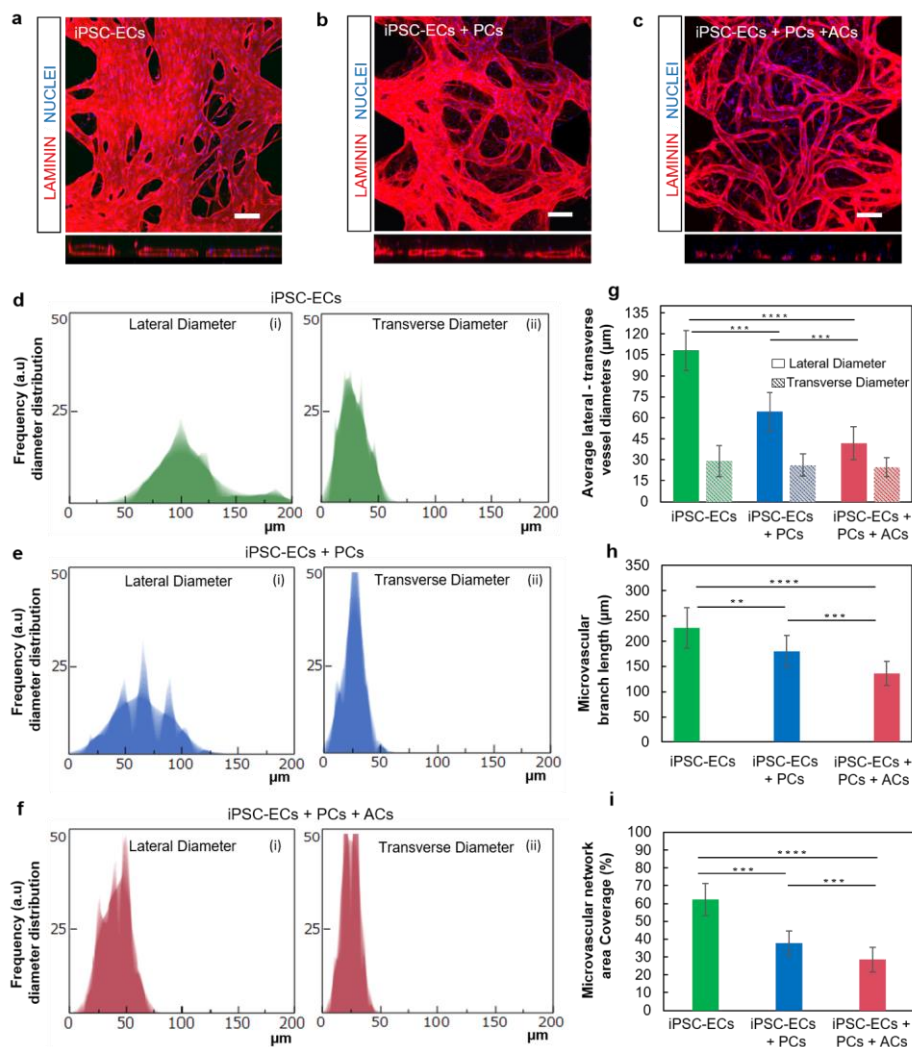


Figure 2: Microvascular network conditions iPSC-ECs - PCs/ACs contact interactions. (a) Schematic representation and (b) confocal images of (a, b, (i)) iPSC-ECs mono-culture (CD31, green), (a, b, (ii)) co-culture with PCs (F-actin, red), and (a, b, (iii)) tri-culture with PCs and ACs (GFAP, magenta), after 7 days of culture in the microfluidic device. (c) Cross-sectional images of blood microvessels showing hollow lumens. (c, (i)) PCs adhered to and partially enveloped brain microvessel. (c, (ii)) Cross-sectional images of blood microvessels showing a lumen enclosed by iPSC-ECs and PCs. PCs surround the blood vessel. Image shows how section was sampled using a line scan measurement (yellow line) and generation of intensity profile histogram. (d) Intensity profile analysis of CD31/F-actin in iPSC-ECs-PCs interaction corresponding to the yellow line scan. Intensity profile shows distinct peaks (yellow arrow) at the position of contact interaction/overlapping between ECs and PCs. CD31 expression (green) was low when F-actin expression (red) was high, further indicating that F-actin expression belonged only to brain PCs outside the vessels. Region of low green intensity corresponds to the vascular bed of the vessel. (e) Contact interactions of PCs enveloping blood microvessel. PCs adhered to and partially enveloped brain microvessel. (f) Confocal image of iPSC-ECs, PCs and ACs in the tri-culture condition. Images were analyzed using Imaris 8.3. Scale bars indicate 100 μm (b) and 20 μm (c, e, f).



334

335 **Figure 3: 3D BBB microvascular network parameter quantification.** Confocal images of laminin
 336 expression (red) and nuclei (DAPI, blue) of 3D BBB μ VN maturation from (a) mono-culture of iPSC-
 337 ECs, (b) co-culture of iPSC-ECs+PCs and (c) tri-culture of iPSC-ECs+PCs+ACs (scale bar: 100 μ m).
 338 Distribution of lateral and transverse vessel diameter measurements of 3D BBB μ VNs formed by
 339 vasculogenesis, for (d) mono-culture of iPSC-ECs, (e) co-culture with brain PCs, (f) tri-culture with
 340 brain PCs and ACs. Additional image in supplementary Fig. 4. (g, h, i) Quantification of
 341 microvascular network parameters: (g) average lateral and transverse vessel diameters in each
 342 condition, (h) microvascular branches average length and (i) percentage ratio of microvascular
 343 network area coverage to the total area. * $p < 0.05$, ** $p < 0.01$, *** $p < 0.001$, **** $p < 0.0001$. Error bars
 344 \pm SD, $n=30$.

Hence, lumens with nearly circular cross-section and consequently smaller cross-section area and higher circularity (Supplementary Fig. 6d-f) formed in the tri-culture condition (average lateral diameter: $42 \pm 13 \mu\text{m}$, average transverse diameter: $25 \pm 6 \mu\text{m}$, Fig. 3g), while lumens were flattened and had elliptical cross-section in mono-cultures (average lateral diameter: $108 \pm 14 \mu\text{m}$, average transverse diameter: $29 \pm 10 \mu\text{m}$, Fig. 3g), and in co-cultures (average lateral diameter: $64 \pm 13 \mu\text{m}$, average transverse diameter: $27 \pm 7 \mu\text{m}$, Fig. 3g).

Moreover, the cumulative average μVN **branch** length decreased from mono-culture ($226 \pm 40 \mu\text{m}$), to co-culture ($179 \pm 31 \mu\text{m}$), and tri-culture ($136 \pm 24 \mu\text{m}$) conditions, respectively (Fig. 3h), demonstrating a highly complex and intertwined vascular network. Accordingly, the networks with iPSC-ECs, iPSC-ECs+PCs, and iPSC-ECs+PCs+ACs conditions covered progressively less area in the projected image (62%, 42%, and 28%, respectively (Fig. 3i). Indeed, in tri-culture conditions, the μVNs showed improved morphology provided by the co-culture with ACs and PCs, with reduced vessel diameters and average branch length. These results mirror similar observations that have been attributed to the secretion of angiogenic growth factors by PCs and ACs [19][20].

In summary, these results indicate that the networks formed with all three cell types --iPSC-ECs+PCs+ACs -- contained more stable and shorter vessel branches, with more circular cross-sections and smaller vessel diameters compared to the other conditions. These networks also exhibited more random interconnections and improved 3D structural orientation into the gel region: such structure is more similar to *in vivo* vessel morphology [30].

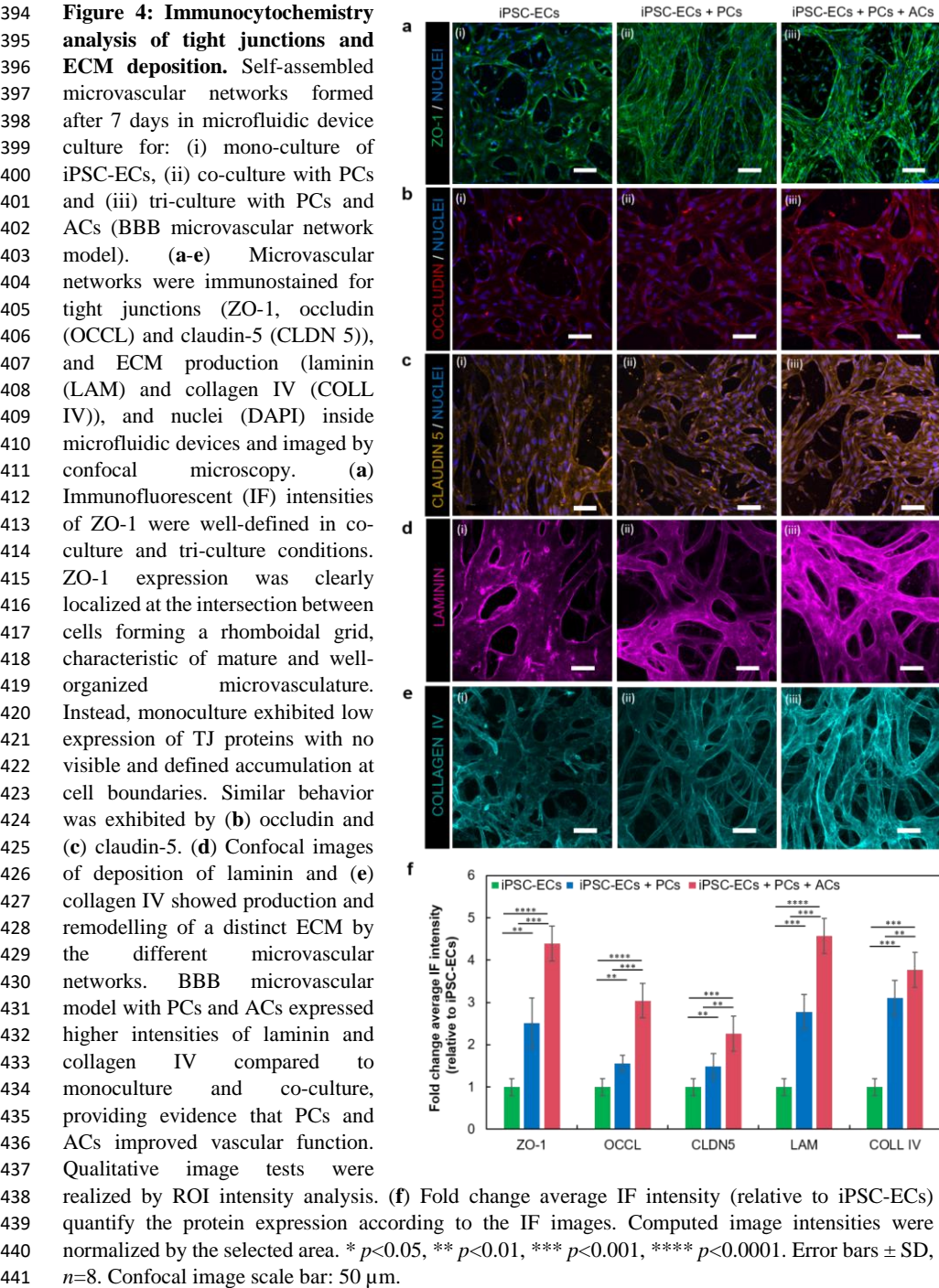
Protein synthesis and gene expression related to blood-brain barrier (BBB)

To analyze whether the engineered 3D brain microvascular model constitutes a functional barrier and exhibits physiological characteristics typical of the BBB present *in vivo*, we validated and compared

protein expression measured by immunocytochemistry assays and quantitative real-time RT-PCR, performed after 7 days. Firstly, immunocytochemistry images of vascular networks obtained under different culture conditions were compared from multiple regions of interest (ROIs) within the vessels. The expression of endothelial-specific junction proteins ZO-1, occludin, and claudin-5 (Fig. 4a-c), and ECM constituents such as laminin (Fig. 4d) and collagen IV (Fig. 4e) was analyzed by confocal microscopy (See also Supplementary fig. 7b-f). Interestingly, the increase of TJ protein expression in μ VNs was observed by introducing PCs and ACs (Fig. 4a-c). Therefore, the BBB μ VNs obtained by iPSC-ECs+PCs+ACs tri-culture (Fig. 4a (iii)) relatively expressed much higher level of ZO-1, occludin and claudin-5 compared to mono-culture of iPSC-ECs and iPSC-ECs+PCs (Fig. 4a-c). Quantitative analysis of fold change average immunofluorescent (IF) intensity (relative to iPSC-ECs) confirmed qualitative observations (Fig. 4f). Average immunofluorescent (IF) intensity was calculated by dividing the total immunofluorescent intensity by the cell boundary length in each ROI in the case of tight-junction proteins (ZO-1, occludin, and claudin-5). In the case of basement membrane protein deposition (laminin, collagen IV), average IF intensity was calculated by dividing the total IF intensity by the vascularized area in each ROI. ROIs were selected to contain only microvascular portions (Fig. 4f). Continuous cell-cell junctions lining the rhomboidal boundaries of endothelial cells along lumens were observed in co-culture and tri-culture conditions, as demonstrated by the clear delineation of ZO-1 along the cell-cell border (Supplementary Fig. 7a).

388

Another sign of vessel maturation was the deposition of basement membrane proteins, exhibiting a similar trend to TJ expression. Laminin and collagen IV immunofluorescence intensity (Fig. 4d-f) approximately doubled in the case of the microvascular networks obtained by iPSC-ECs+PCs+ACs tri-culture (Fig. 4d,e (iii)) compared to iPSC-ECs mono-culture (Fig. 4d,e (i)) and was significantly higher than for iPSC-ECs+PCs co-culture (Fig. 4d,e (ii)).



442 To confirm immunocytochemistry results, total RNA was extracted from the total cell population in
443 the microfluidic device (Fig. 5a) and purified from different conditions at several time points (day 0,
444 4, and 7). RT-PCR analysis was conducted considering gene markers of TJ proteins, ECM production
445 and several endothelial membrane transporters such as efflux-pumps, passive transports, solute
446 carriers, and receptor-mediated mechanisms. Vessel maturation was investigated in terms of the
447 expression of several markers and proteins, in the case of co-culture and tri-culture conditions, and
448 was compared to the control condition (iPSC-ECs). The mRNA expression of each gene was
449 measured relative to the expression of CD31 and GAPDH (fold change). TJ proteins such as ZO-1,
450 occludin, and claudin-5 were highly up-regulated in the tri-culture condition at day 7 compared to
451 mono-culture and co-culture conditions. Interestingly, the expression of TJ markers in the tri-culture
452 case increased as a function of culture time (Fig. 5b, Supplementary Fig. 10a-e). As expected, GFAP
453 was regulated exclusively in the presence of ACs. PDGFR gene expression was slightly higher in the
454 tri-culture condition while alpha-smooth muscle actin (α SMA) expression was reduced, possibly due
455 to the increased proliferation of iPSC-ECs and PCs stimulated by ACs. Furthermore, basement
456 membrane proteins (collagen IV, laminin) were highly expressed over time in the tri-culture condition
457 compared to the mono- and co-culture cases. In addition, gene expression of several BBB-specific
458 membrane transporters and receptors which exploit several transport mechanisms (passive diffusion,
459 ATP-binding efflux transporter, solute carriers and receptor-mediated transcytosis), such as P-GP,
460 MRP1, MRP4, TF-R, LRP1, LAT-1, GLUT-1, CAT1, MCT1, ABCA1, and BCRP widely increased
461 over time in the tri-culture BBB model (iPSC-ECs+PCs+ACs), compared to iPSC-ECs+PCs and
462 iPSC-ECs microvascular network conditions. Overall after 7 days, the tri-culture condition displayed
463 a constantly increased maturation and upregulation of all examined genes (Fig. 5b, Supplementary
464 Fig. 10a-e, Primer sequences in Supplementary Table 1).

465

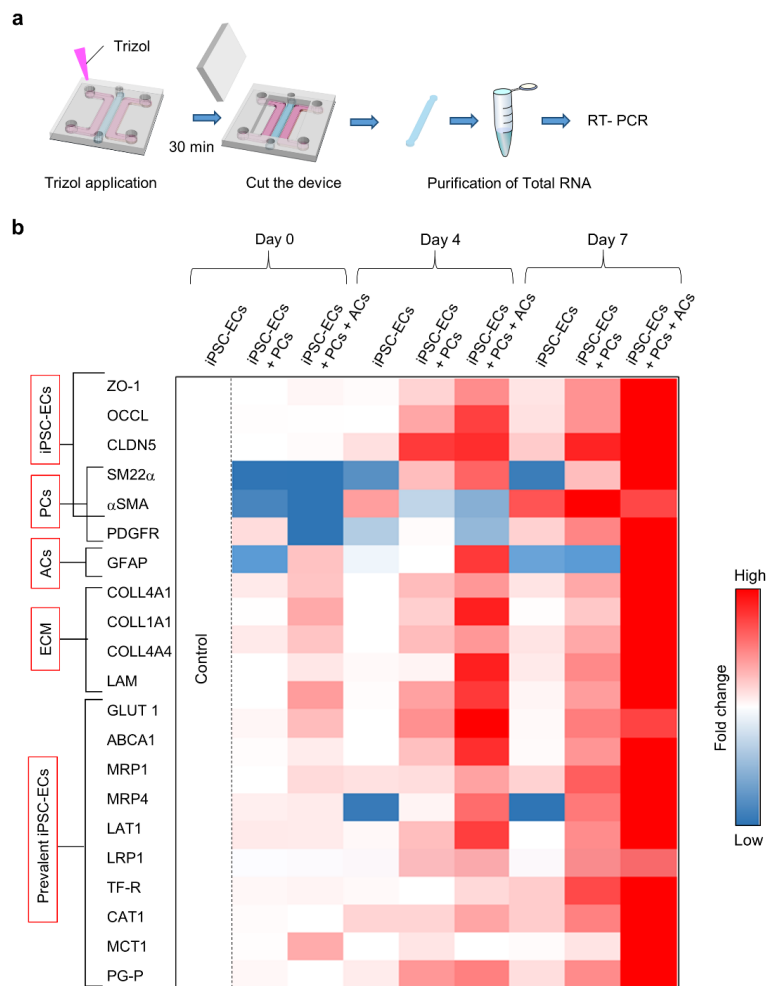
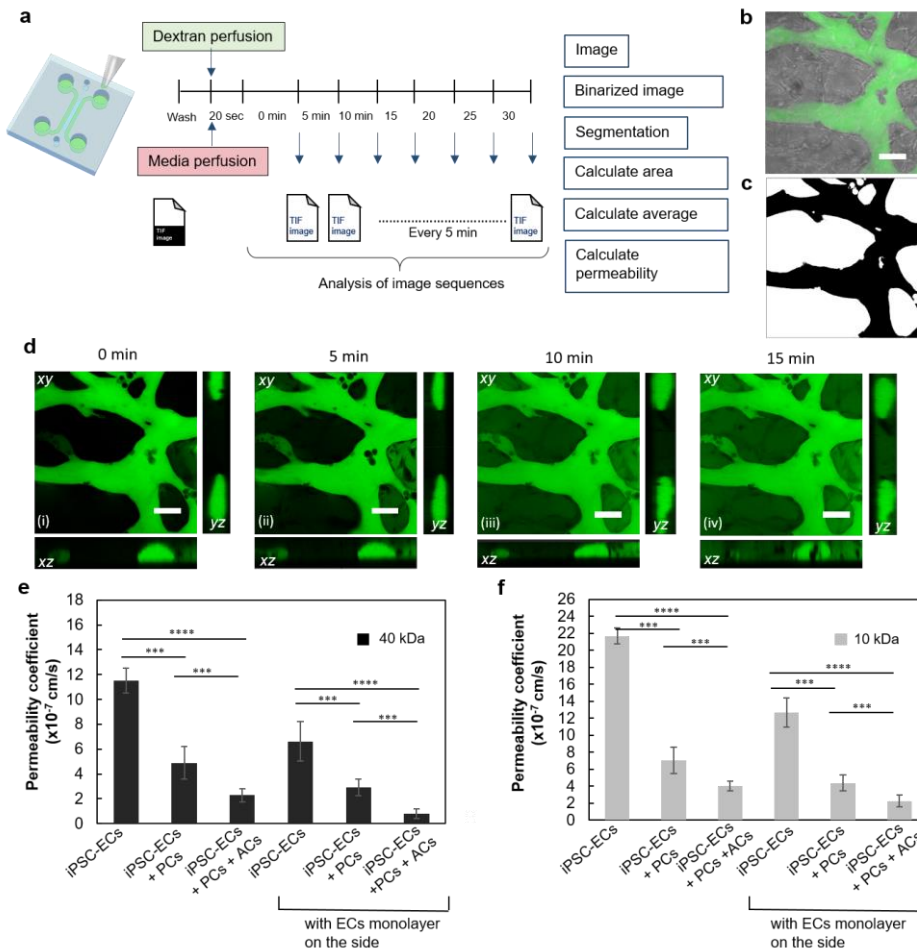


Figure 5: Quantitative relative RT-PCR of 3D BBB μ VNs in microfluidic device. (a) Schematic representation of vascular network and gel extraction from a microfluidic device, purification of total RNA and conduct of RT-PCR experiments. (b) Heatmap of RT-PCR results of mono-culture of iPSC-ECs, co-culture with PCs, and tri-culture with PCs and ACs at 0, 4 and 7 days. Relative comparison of mRNA expression of factors relating to microvascular maturation and other typical BBB features. Gene analysis considered markers 1) expressed in ECs, 2) expressed in PCs, 3) expressed in ACs, 4) ECM protein RNA, and 5) genes expressed predominantly by ECs, but also in smaller amounts by the other two cell types. Fold change was relative to control (mono-culture of iPSC-ECs, day 0). The internal standard housekeeping gene was CD31. $0.01 < p < 0.05$, $n = 3$.

475 **Distinct cell contributions to BBB permeability**

476 The permeability of the microvessels in our BBB μ VN models was computed to assess the practical
477 potential to use our system to mimic solute transport *in vivo*. In all culture conditions, vessels
478 comprising the entire vascular network were well formed and completely perfusable at day 7
479 (Supplementary Fig. 8d, Supplementary video 2, 3). Permeability coefficients were measured by
480 introducing solutions containing FITC-dextran tracers in the vasculature (10 & 40 kDa), and
481 capturing confocal images at 5 min intervals and computing them as explained in Methods (Fig.
482 6a-d, Supplementary Fig. a-c). With side-channels seeded with iPSC-ECs, permeability to 40 kDa
483 FITC-dextran of the μ VN obtained under mono-, co-, and tri-culture conditions progressively
484 decreased: 6.6, 2.5, and 0.89×10^{-7} cm/s, respectively. A similar trend was observed for the 10 kDa
485 FITC-dextran: 12, 4.8 and 2.2×10^{-7} cm/s, respectively (Fig. 6e, f). When iPSC-ECs were not added
486 to the side channels, leakage of tracer across the side-walls of the gel region gave rise to higher
487 permeability values, roughly a two-fold increase, due to the artifact associated with the additional
488 source of tracer influx. Side channel seeding helped in several ways. It improved coverage of the
489 exposed side gel surface with an endothelial monolayer, filled gaps that sometimes formed at the gel-
490 post borders, and increased the number and patency of connections between the networks and the
491 main channel (Fig. 7a and Supplementary Fig. 9a-e).

492



493

494 **Figure 6: Permeability assay in BBB model.** (a) Timeline of permeability experiments and
 495 computational analysis. After cell culture medium was removed, dextran solution was injected and
 496 image stacks were captured every 3-5 mins for 30 mins. Workflow of image analysis by ImageJ and
 497 permeability coefficient calculation. (b) Confocal and bright field images at time 0. (c) Image
 498 binarization after thresholding to identify vessel borders. (d, i-iv) Maximum image projections and
 499 cross-sections including xy, xz and yz planes at 4 time-points. The graphs show permeability
 500 coefficients for 3 different conditions (with and without ECs seeding in side channels) using (e) 40
 501 kDa and (f) 10 kDa FTIC-dextran in mono-culture of iPSC-ECs, co-culture of iPSC-ECs+PCs, and
 502 tri-culture of iPSC-ECs+PCs+ACs. The data show mean value, error bars \pm SD, $n=10$, * $p<0.05$, **
 503 $p<0.01$, *** $p<0.001$, **** $p<0.0001$, scale bars 50 μ m.

a

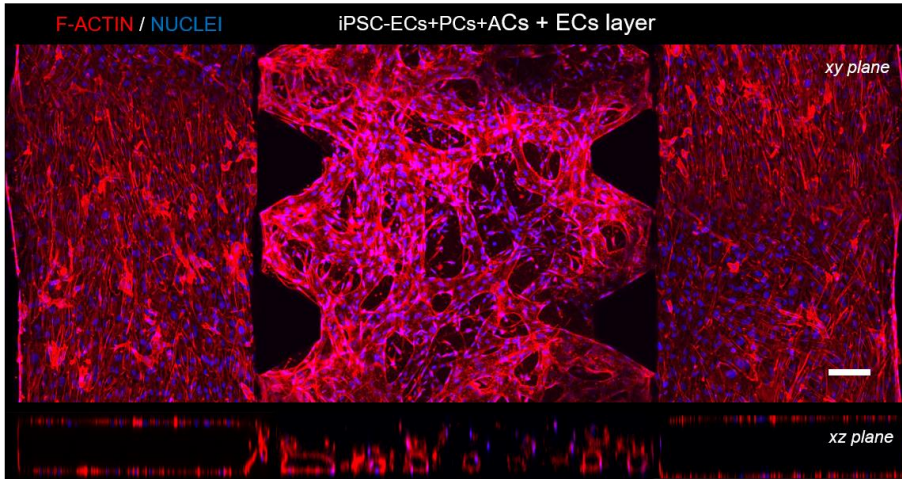


Figure 7: BBB microvascular network model. (a) Confocal images of xy and xz (cross-section) planes of the 3D BBB microvascular *in vitro* model with iPSC-ECs+PCs+ACs, including EC layers in the side channel. Scale bars 200 μm .

508 Discussion

509

510 In this work, we developed a new *in vitro* human BBB microvascular model consisting of a self-
511 assembled μ VN of iPSC-ECs co-cultured with brain PCs and ACs. Novelty of our microfluidic
512 platform arises from simultaneous seeding of three human cell types into a single gel region,
513 producing a perfusable vascular network, with permeabilities lower than those of other published
514 microfluidic models [23][24][27][32][34].

515

516 iPSC-ECs were selected as they are immature endothelial cells, capable of organizing into a complex
517 and perfusable vascular network [41], with lower permeability values compared to other non-brain
518 EC models [42][43][44]. The potential features of iPSC-ECs may contribute to a coherent and
519 relevant replacement of “brain” endothelial cells to establish a 3D BBB microvascular model.
520 Moreover, iPS cells may be potentially derived from patients who suffer from specific
521 neurodegenerative diseases [45], thereby producing a pathological model to study disease progression,
522 to screen for drugs appropriate for patients’ sub-groups, or even for precision medicine applications
523 to select optimal, personalized therapies.

524

525 Our 3D BBB μ VN model incorporating three cell-types (Fig. 1b and Fig. 7a) expressed both
526 functional and morphological characteristics present in the human BBB, with stable and perfusable
527 μ VNs, comprising small lumens with circular cross-section comparable with *in vivo* human
528 microcirculation (arterioles and venules $<100\ \mu\text{m}$; capillaries $<10\ \mu\text{m}$) [28][29]. It also defined
529 microvascular branch length similar to segments in close proximity to the third ventricle (caudate,
530 putamen, and thalamus with an average of $70\ \mu\text{m}$) [46] and characterized by low permeability and
531 transport selectivity (Fig. 6e,f and Supplementary movie 2, 3). It draws upon the intrinsic nature of
532 ECs interacting with other neural cell types to recapitulate brain vascular morphogenesis during
533 developmental process via vasculogenesis [47][48], in which immature ECs recruit PCs and ACs to

534 form new vessels through PDGFR and Sonic hedgehog (SHH) signaling pathways [47][49]. In
535 particular, PCs played an important role to create a robust and stable vessel network with significant
536 lateral diameter reduction (Fig. 3d,g). It has been previously demonstrated that ECs need a
537 combination of juxtacrine and paracrine signaling to create a stable and physiologically-relevant
538 microvasculature on a chip [38][39]. Hence, the resulting formation of a physiologically-relevant
539 microvasculature, was facilitated by juxtacrine interactions and paracrine signaling between iPSC-
540 ECs and PCs (enveloping the endothelium) (Fig. 2c-e), along with the increase of TJ expression and
541 appropriate concentration of growth factors (Fig. 4a-c, Supplementary Figs. 7a-d, 10a-d). Indeed,
542 improvements were associated with the presence and secretion of vascular endothelial growth factor
543 VEGF (50 ng/ml in the supplemented medium), angiopoietin-1 (ANG-1) and fibroblast growth factor
544 (FGF) by stromal cells, especially PCs [50]. However, as VEGF could modulate vascular
545 permeability through the disruption of tight junctions and consequent break down of the BBB [51],
546 cell culture medium was supplemented with VEGF up to day 4.

547
548 We hypothesize that this morphological change in the final structure of the BBB μ VNs was induced
549 by not only the presence and cell-secretion of pro-angiogenic and vasculogenic growth factors and
550 ECM proteins, but also by juxtacrine signaling, consistent with previous findings [35][52][53]. Our
551 results also suggest that PCs not only influence the creation of vascular networks but also induce the
552 differentiation of iPSC-ECs into brain-specific endothelial cells, as determined by the RT-PCR results
553 (Fig. 5b, Supplementary Fig. 10a-d). Indeed, it has already been shown that co-culture of ECs with
554 PCs is required for BBB formation and the maintenance of homeostasis by contact and paracrine
555 interactions [54].

556
557 In addition to the contribution of PCs, ACs also improved BBB formation and integrity. iPSC-ECs
558 self-assembled into mature vascular networks forming complex structures when interacting with both
559 cell types. The role of ACs was evidenced by an increase in the expression of BBB transporters and

560 TJ proteins, such as ZO-1, occludin, claudin-5, ECM deposition (Figs. 4a-e, 5b, Supplementary Fig.
561 7a-c), and the corresponding decrease in permeability, (Fig. 6e-f) similar to previous transwell and
562 microfluidic-based models incorporating ACs [55]. In particular, the upregulation of typical BBB
563 transporters such GLUT-1, LAT-1, PG-P, TF-R, LRP1 and MRPs is fundamental to obtain an *in vitro*
564 BBB model for drug design and testing. Indeed, these specific transporters were highlighted as
565 potential targets to enhance the penetration of drugs into the brain [56] (Supplementary Fig. 10d).

566

567 In our model, AC endfeet were directly attached to the surface of vascular networks in the 3D matrix
568 (Fig. 2f, Supplementary Fig. 6b,c). This morphological feature of ACs recapitulates their
569 physiological arrangement in the brain and provides mutual biochemical support for those cells,
570 helping to maintain the integrity of the neurovascular networks [57]. Our findings suggest that the
571 addition of ACs is in part responsible for the improved morphology of BBB anatomical structure.
572 They might also contribute through paracrine signals to the development of a BBB-like endothelial
573 phenotype since ACs are known to regulate influx/efflux, vasodilatation/vasoconstriction by inducing
574 tightening of the endothelium [19], as well as cytokine and growth factor secretion such as basic FGF,
575 glial-derived neurotrophic factor (GDNF), and ANG-1 [58]. Further investigation is needed to
576 ascertain the relative importance of different biological pathways and factors improving BBB
577 integrity, however, direct adhesion of ECs, PCs and ACs might facilitate N-cadherin cell-cell
578 interactions [47].

579

580 As key features in assessing the value of BBB microvascular models for drug transport studies,
581 vascular perfusability and permeability were measured using fluorescent probes. The vessel networks
582 in our tri-culture BBB model attained permeability values of 8.9×10^{-8} cm/s and 2.2×10^{-7} cm/s for 40
583 kDa and 10 kDa FITC-dextran, respectively (Fig. 6e,f), confirming barrier selectivity depending on
584 their molecular weight [59].

585 Importantly, these values are comparable to those measured *in vivo* in rat cerebral microcirculation

586 (3.1 ± 1.3×10⁻⁷ cm/s for a 10 kDa FITC-dextran) [60], (1.37± 0.26×10⁻⁷ cm/s for a 40 kDa FITC-
587 dextran) [61], and similar to specific models that employ brain ECs derived from iPSCs (IMR90-4)
588 by co-culturing with astrocytes and/or neurons [62][63], and lower than previously reported 3D
589 [23][27][32][34], or 2D BBB models [24][64].

590

591 As a side note, inclusion of an iPSC-EC monolayer in the adjacent fluidic channels improved vascular
592 perfusability and also reduced the artifacts associated with tracer leakage across the sidewalls of the
593 gel region (Fig. 7, Supplementary Fig. 9a-e). Consistent with the progressive reduction in
594 permeability with increasing model complexity, we observed a corresponding increase in the tightness
595 of junctional proteins and their regulation [53][65], evaluated by immunostaining and RT-PCR
596 analysis. This contrasts with a previous study that reported an increase in permeability coefficient
597 when human brain endothelial cells (hCMEC/d3) were co-cultured with ACs isolated from rats [32],
598 possibly due to cross-species effects, as suggested by the authors of [29].

599

600 It is important to note that our model lacked neurons and microglia, and these might have further
601 effects on barrier functionality. Recent literature has shown that the upregulation of BBB-specific
602 transporters and the differentiation of brain-specific ECs are induced by the co-culture of iPSC-ECs
603 with iPS derived neurons [66]. In the same model authors demonstrated the possibility of drug
604 screening using iPSC-ECs in combination with all human iPS derived cells using transwell methods.
605 Also, co-culture with neural iPSCs has been found to improve EC barrier integrity and decrease
606 vascular permeability [66]. Therefore, there appear to be additional advantages gained by an even
607 more comprehensive human patient-derived *in vitro* model [66], combining iPSCs and/or neural stem
608 cells with the vascular networks, PCs, and ACs described here. Moreover, using iPS cells derived
609 from patients affected by neurological disorders [45], such as Alzheimer's disease, a BBB
610 pathological model could be obtained.

611

612 Our 3D self-organized system has several advantages compared to the *in vitro* 2D membrane-based
613 monolayer, including its more physiologically-relevant morphology. Permeability measurements,
614 however, at this point are limited to quantifying concentrations of a fluorescent tracer. Similar
615 measurements could be made by tagging the molecule of interest with a fluorescent marker using this
616 same experimental protocol. Alternatively, samples of interstitial fluid could be directly collected
617 from the gel filling ports in the device, and used to quantify transport into the matrix, but this could
618 be problematic due to the low drug concentrations in the gel region.

619 Although PDMS is widely used for microfluidic applications, one of its disadvantages is non-specific
620 adsorption of proteins and small hydrophobic molecules during long-term interaction [67]. Even
621 though this would not have affected our current permeability study, in perspective of drug testing,
622 several treatments exist to prevent fouling of the PDMS surface. Accordingly, distinct surface
623 modifications that could reduce non-specific absorption include coating the PDMS surface with
624 bovine serum albumin (BSA) [68], grafting with anti-fouling molecules [69], or silanization [70].

625

626 Other possible improvements to the current model are the introduction of continuous perfusion to
627 improve microvascular formation and reduce vascular permeability in the perspective of a long-term
628 culture system. Indeed, flow perfusion culture could advance the model in two important aspects.
629 Firstly, oxygen and glucose transport into the vessels will tend to modulate glycolytic metabolism in
630 favor of the more efficient aerobic respiration useful for maintaining a long-term culture. Secondly,
631 flow-mediated shear stress is known to promote the differentiation of vascular endothelial cells into
632 a more BBB-like phenotype with the highest expression of TJ proteins and membrane transporters,
633 producing further reductions in permeability [71]. Finally, it would be beneficial to assess the trans-
634 endothelial electrical resistance (TEER) measurement as another metric of BBB function [24].

635

636 **Conclusion**

637

638 Here we present the first highly functional 3D BBB *in vitro* model produced by vasculogenesis that
639 incorporate human iPSC-ECs microvascular network in contact interaction with human brain PCs
640 and ACs within a single 3D ECM/fibrin gel region. Our 3D BBB microvascular model exhibits
641 physiologically relevant structures and provides an effective and reproducible platform compared to
642 static models [16][17], useful in the study of dynamic transport of small and large molecules across
643 the BBB in a complex microenvironment [72]. We believe this is a reliable and valuable next-
644 generation system that furthers the understanding of neurovascular function, enables the preclinical
645 development of effective CNS therapeutics [16], can be applied to probe metastatic cancer
646 extravasation [26][73] and evaluate reciprocal brain-systemic circulation interactions that occur in
647 inflammatory and neurodegenerative diseases [4-9]. This translational model could be adapted for the
648 high-throughput pre-clinical screening of innovative therapies targeting specific BBB transporters, to
649 perform drug delivery studies and to investigate the transport of microengineered nanocarriers able
650 to cross the BBB.

References

- [1] N. J. Abbott, "Dynamics of CNS barriers: Evolution, differentiation, and modulation," *Cell. Mol. Neurobiol.*, vol. 25, no. 1, pp. 5–23, 2005.
- [2] N. J. Abbott, A. A. K. Patabendige, D. E. M. Dolman, S. R. Yusof, and D. J. Begley, "Structure and function of the blood-brain barrier," *Neurobiol. Dis.*, vol. 37, no. 1, pp. 13–25, 2010.
- [3] Y. Serlin, I. Shelef, B. Knyazer, and A. Friedman, "Anatomy and physiology of the blood-brain barrier," *Semin. Cell Dev. Biol.*, vol. 38, pp. 2–6, 2015.
- [4] R. D. B. V. Zlokovic, "Neurovascular mechanisms and blood–brain barrier disorder in Alzheimer’s disease," *Acta Neuropathol.*, vol. 36, no. 3, pp. 490–499, 2010.
- [5] B. V. Zlokovic, "Neurovascular mechanisms of Alzheimer’s neurodegeneration," *Trends Neurosci.*, vol. 28, no. 4, pp. 202–208, 2005.
- [6] R. Kortekaas *et al.*, "Blood-brain barrier dysfunction in Parkinsonian midbrain in vivo," *Ann. Neurol.*, vol. 57, no. 2, pp. 176–179, 2005.
- [7] E. Waubant, "Biomarkers indicative of blood-brain barrier disruption in multiple sclerosis.," *Dis. Markers*, vol. 22, no. 4, pp. 235–244, 2006.
- [8] R. K. Jain, E. Di Tomaso, D. G. Duda, J. S. Loeffler, A. G. Sorensen, and T. T. Batchelor, "Angiogenesis in brain tumours," *Nat. Rev. Neurosci.*, vol. 8, no. 8, pp. 610–622, 2007.
- [9] B. T. Hawkins and T. P. Davis, "The Blood-Brain Barrier / Neurovascular Unit in Health and Disease," *Pharmacol. Rev.*, vol. 57, no. 2, pp. 173–185, 2005.
- [10] W. M. Pardridge, "CSF, blood-brain barrier, and brain drug delivery.," *Expert Opin. Drug Deliv.*, vol. 5247, no. May, pp. 1–13, 2016.
- [11] W. M. Pardridge, "Why is the global CNS pharmaceutical market so under-penetrated?," *Drug Discov. Today*, vol. 7, no. 1, pp. 5–7, 2002.
- [12] W. M. Pardridge, "Blood-brain barrier drug targeting: the future of brain drug development.," *Mol. Interv.*, vol. 3, no. 2, pp. 90–105, 51, 2003.
- [13] N. J. Abbott, "Prediction of blood–brain barrier permeation in drug discovery from in vivo, in vitro and in silico models," *Drug Discov. Today Technol.*, vol. 1, no. 4, pp. 407–416, Dec. 2004.
- [14] D. Pamies, T. Hartung, and H. T. Hogberg, "Biological and medical applications of a brain-on-a-chip.," *Exp. Biol. Med. (Maywood).*, pp. 1096–1107, 2014.
- [15] P. S., "Preclinical research: Make mouse studies work," *Nature*, vol. 507, no. 425, 2014.
- [16] R. Cecchelli *et al.*, "Modelling of the blood–brain barrier in drug discovery and development," *Nat. Rev. Drug Discov.*, vol. 6, no. 8, pp. 650–661, 2007.
- [17] M. W. van der Helm, A. D. van der Meer, J. C. T. Eijkel, A. van den Berg, and L. I. Segerink, "Microfluidic organ-on-chip technology for blood-brain barrier research.," *Tissue barriers*, vol. 4, no. 1, p. e1142493, 2016.

- 687 [18] K. Hatherell, P. O. Couraud, I. A. Romero, B. Weksler, and G. J. Pilkington, "Development of a
688 three-dimensional, all-human in vitro model of the blood-brain barrier using mono-, co-, and tri-
689 cultivation Transwell models," *J. Neurosci. Methods*, vol. 199, no. 2, pp. 223–229, 2011.
- 690 [19] N. J. Abbott, L. Rönnbäck, and E. Hansson, "Astrocyte-endothelial interactions at the blood-brain
691 barrier," *Nat. Rev. Neurosci.*, vol. 7, no. 1, pp. 41–53, 2006.
- 692 [20] M. D. Sweeney, S. Ayyadurai, and B. V. Zlokovic, "Pericytes of the neurovascular unit: key functions
693 and signaling pathways," *Nat. Neurosci.*, vol. 19, no. 6, pp. 771–783, 2016.
- 694 [21] C. F. Cho *et al.*, "Blood-brain-barrier spheroids as an in vitro screening platform for brain-penetrating
695 agents," *Nat. Commun.*, vol. 8, pp. 1–14, 2017.
- 696 [22] E. Urich, C. Patsch, S. Aigner, M. Graf, R. Iacone, and P. O. Freskgård, "Multicellular self-assembled
697 spheroidal model of the blood brain barrier," *Sci. Rep.*, vol. 3, 2013.
- 698 [23] J. D. Wang, E. S. Khafagy, K. Khanafer, S. Takayama, and M. E. H. Elsayed, "Organization of
699 Endothelial Cells, Pericytes, and Astrocytes into a 3D Microfluidic in Vitro Model of the Blood-Brain
700 Barrier," *Mol. Pharm.*, vol. 13, no. 3, pp. 895–906, 2016.
- 701 [24] R. Booth and H. Kim, "Characterization of a microfluidic in vitro model of the blood-brain barrier
702 (μ BBB)," *Lab Chip*, vol. 12, no. 10, p. 1784, 2012.
- 703 [25] H. Cho *et al.*, "Three-Dimensional Blood-Brain Barrier Model for in vitro Studies of Neurovascular
704 Pathology," *Sci. Rep.*, vol. 5, p. 15222, 2015.
- 705 [26] H. Xu *et al.*, "A dynamic in vivo-like organotypic blood-brain barrier model to probe metastatic brain
706 tumors," *Sci. Rep.*, vol. 6, no. 1, p. 36670, 2016.
- 707 [27] A. Herland, A. D. van der Meer, E. A. FitzGerald, T.-E. Park, J. J. F. Sleeboom, and D. E. Ingber,
708 "Distinct Contributions of Astrocytes and Pericytes to Neuroinflammation Identified in a 3D Human
709 Blood-Brain Barrier on a Chip," *PLoS One*, vol. 11, no. 3, p. e0150360, 2016.
- 710 [28] I. M. Braverman, "The Cutaneous Microcirculation," *J. Investig. Dermatology Symp. Proc.*, vol. 5,
711 no. 1, pp. 3–9, 2000.
- 712 [29] A. D. Wong, M. Ye, A. F. Levy, J. D. Rothstein, D. E. Bergles, and P. C. Searson, "The blood-brain
713 barrier: an engineering perspective," *Front. Neuroeng.*, vol. 6, no. August, pp. 1–22, 2013.
- 714 [30] T. Takano *et al.*, "Astrocyte-mediated control of cerebral blood flow.," *Nat. Neurosci.*, vol. 9, no. 2,
715 pp. 260–267, 2006.
- 716 [31] K. Kisler, A. R. Nelson, A. Montagne, and B. V. Zlokovic, "Cerebral blood flow regulation and
717 neurovascular dysfunction in Alzheimer disease," *Nat. Rev. Neurosci.*, vol. 18, no. 7, pp. 419–434,
718 2017.
- 719 [32] G. Adriani, D. Ma, A. Pavesi, and R. D. Kamm, "A 3D neurovascular microfluidic model consisting
720 of neurons, astrocytes and cerebral endothelial cells as a blood–brain barrier," *Lab Chip*, vol. 12, pp.
721 169–182, 2017.
- 722 [33] J. A. Whisler, M. B. Chen, and R. D. Kamm, "Control of perfusable microvascular network

morphology using a multiculture microfluidic system.,” *Tissue Eng. Part C. Methods*, vol. 20, no. 7, pp. 543–52, 2014.

[34] S. Bang *et al.*, “A Low Permeability Microfluidic Blood-Brain Barrier Platform with Direct Contact between Perfusable Vascular Network and Astrocytes,” *Sci. Rep.*, vol. 7, no. 1, p. 8083, 2017.

[35] E. a Winkler, R. D. Bell, and B. V Zlokovic, “Central nervous system pericytes in health and disease.,” *Nat. Neurosci.*, vol. 14, no. 11, pp. 1398–1405, 2011.

[36] Y. Shin *et al.*, “Reconstituting vascular microenvironment of neural stem cell niche in three-dimensional extracellular matrix,” *Adv. Healthc. Mater.*, vol. 3, no. 9, pp. 1457–1464, 2014.

[37] Y. Shin *et al.*, “Microfluidic assay for simultaneous culture of multiple cell types on surfaces or within hydrogels,” *Nat. Protoc.*, vol. 7, no. 7, pp. 1247–1259, 2012.

[38] A. Hasan *et al.*, “Microfluidic techniques for development of 3D vascularized tissue,” *Biomaterials*, vol. 35, no. 26, pp. 7308–7325, 2014.

[39] K. Haase and R. D. Kamm, “Advances in on-chip vascularization.,” *Regen. Med.*, vol. 12, no. 3, pp. 285–302, 2017.

[40] F. E. Curry, V. H. Huxley, and R. H. Adamson, “Permeability of single capillaries to intermediate-sized colored solutes.,” *Am. J. Physiol.*, vol. 245, no. 3, pp. H495-505, 1983.

[41] D. G. Belair *et al.*, “Human vascular tissue models formed from human induced pluripotent stem cell derived endothelial cells,” *Stem Cell Rev. Reports*, vol. 11, no. 3, pp. 511–525, 2015.

[42] S. Kim, H. Lee, M. Chung, and N. L. Jeon, “Engineering of functional, perfusable 3D microvascular networks on a chip,” *Lab Chip*, vol. 13, no. 8, pp. 1489–1500, 2013.

[43] and R. D. K. Michelle B. Chen, Jordan A. Whisler , Jessie S. Jeon, “Mechanisms of tumor cell extravasation in an in vitro microvascular network platform,” *Integr. Biol.*, vol. 144, no. 5, pp. 724–732, 2014.

[44] J. S. Jeon *et al.*, “Generation of 3D functional microvascular networks with human mesenchymal stem cells in microfluidic systems,” *Integr. Biol.*, vol. 6, no. 5, pp. 555–563, 2014.

[45] T. Osaki, Y. Shin, V. Sivathanu, M. Campisi, and R. D. Kamm, “In Vitro Microfluidic Models for Neurodegenerative Disorders,” *Adv. Healthc. Mater.*, vol. 1700489, p. 1700489, 2017.

[46] P. Kreczmanski *et al.*, “Microvessel length density, total length, and length per neuron in five subcortical regions in schizophrenia,” *Acta Neuropathol.*, vol. 117, no. 4, pp. 409–421, 2009.

[47] B. Obermeier, R. Daneman, and R. M. Ransohoff, “Development, maintenance and disruption of the blood-brain-barrier,” *Nat. Med.*, vol. 19, no. 12, pp. 1584–1596, 2013.

[48] N. Hagan and A. Ben-Zvi, “The molecular, cellular, and morphological components of blood-brain barrier development during embryogenesis,” *Semin. Cell Dev. Biol.*, vol. 38, pp. 7–15, 2015.

[49] R. Daneman, L. Zhou, A. A. Kebede, and B. A. Barres, “Pericytes are required for blood-brain barrier integrity during embryogenesis,” *Nature*, vol. 468, no. 7323, pp. 562–566, 2010.

[50] G. Bergers and S. Song, “The role of pericytes in blood-vessel formation and maintenance.,” *Neuro.*

Oncol., vol. 7, no. 4, pp. 452–464, 2005.

[51] M. A. Proescholdt *et al.*, “Vascular endothelial growth factor (VEGF) modulates vascular permeability and inflammation in rat brain,” *J. Neuropathol. Exp. Neurol.*, 1999.

[52] J. Kim, M. Chung, S. Kim, D. H. Jo, J. H. Kim, and N. L. Jeon, “Engineering of a biomimetic pericyte-covered 3D microvascular network,” *PLoS One*, vol. 10, no. 7, pp. 1–15, 2015.

[53] R. C. Brown, A. P. Morris, and R. G. O’Neil, “Tight junction protein expression and barrier properties of immortalized mouse brain microvessel endothelial cells,” *Brain Res.*, vol. 1130, no. 1, pp. 17–30, 2007.

[54] M. D. Sweeney, S. Ayyadurai, and B. V. Zlokovic, “Pericytes of the neurovascular unit: key functions and signaling pathways,” *Nat. Neurosci.*, vol. 19, no. 6, pp. 771–83, 2016.

[55] B. Prabhakarparandian *et al.*, “SyM-BBB: a microfluidic Blood Brain Barrier model,” *Lab Chip*, vol. 13, no. 6, pp. 1093–1101, 2013.

[56] W. Löscher and H. Potschka, “Blood-brain barrier active efflux transporters: ATP-binding cassette gene family,” *NeuroRX*, vol. 2, no. 1, pp. 86–98, 2005.

[57] S. Banerjee and M. A. Bhat, “Neuron-Glial Interactions in Blood-Brain Barrier Formation,” *Annu. Rev. Neurosci.*, vol. 30, pp. 235–258, 2007.

[58] S.-W. Lee *et al.*, “SSeCKS regulates angiogenesis and tight junction formation in blood-brain barrier,” *Nat. Med.*, vol. 9, no. 7, pp. 900–906, 2003.

[59] D. J. Begley, “Delivery of therapeutic agents to the central nervous system: the problems and the possibilities,” *Pharmacol. Ther.*, vol. 104, no. 1, pp. 29–45, 2004.

[60] W. Yuan, Y. Lv, M. Zeng, and B. M. Fu, “Non-invasive measurement of solute permeability in cerebral microvessels of the rat,” *Microvasc. Res.*, vol. 77, no. 2, pp. 166–173, Mar. 2009.

[61] S. Y. Shi L., Zeng M., “Quantification of Blood-Brain Barrier Solute Permeability and Brain Transport by Multiphoton Microscopy,” vol. 136, no. March 2014, pp. 1–9, 2014.

[62] Y. I. Wang, H. E. Abaci, and M. L. Shuler, “Microfluidic blood-brain barrier model provides in vivo-like barrier properties for drug permeability screening,” *Biotechnol. Bioeng.*, vol. 114, no. 1, pp. 184–194, 2017.

[63] S. G. Canfield *et al.*, “An isogenic blood-brain model comprising brain endothelial cells, astrocytes and neurons derived from human induced pluripotent stem cells,” *Neurochem. J. O F*, no. 140, pp. 874–888, 2017.

[64] J. M. Guanglei Li, Melissa J. Simon, Limary M. Cancel, Zhong-Dong Shi, Xinying Ji and B. M. F. Tarbell, Barclay Morrison, “Permeability of Endothelial and Astrocyte Cocultures: In Vitro Blood–Brain Barrier Models for Drug Delivery Studies,” *Annu. Biomed. Eng.*, vol. 38, no. 8, pp. 2499–2511, 2010.

[65] J. D. Huber, K. A. Witt, S. Hom, R. D. Egleton, K. S. Mark, and T. P. Davis, “Inflammatory pain alters blood-brain barrier permeability and tight junctional protein expression,” *Am. J. Physiol. Heart*

Circ. Physiol., vol. 280, no. 3, pp. H1241–H1248, 2001.

[66] A. Appelt-Menzel *et al.*, “Establishment of a Human Blood-Brain Barrier Co-culture Model Mimicking the Neurovascular Unit Using Induced Pluri- and Multipotent Stem Cells,” *Stem Cell Reports*, vol. 8, no. 4, pp. 894–906, 2017.

[67] M. W. Toepke and D. J. Beebe, “PDMS absorption of small molecules and consequences in microfluidic applications,” *Lab Chip*, no. c, pp. 1484–1486, 2006.

[68] E. Ostuni, C. S. Chen, D. E. Ingber, and G. M. Whitesides, “Selective Deposition of Proteins and Cells in Arrays of Microwells,” *Langmuir*, vol. 17, no. 9, pp. 2828–2834, 2001.

[69] A. Gokaltun, M. L. Yarmush, A. Asatekin, and O. B. Usta, “Recent advances in nonbiofouling PDMS surface modification strategies applicable to microfluidic technology,” *Technology*, vol. 5, no. 1, pp. 1–12, 2017.

[70] S. Jon, J. Seong, A. Khademhosseini, T. T. Tran, P. E. Laibinis, and R. Langer, “Construction of Nonbiofouling Surface by Polymeric Self-Assembled Monolayers,” *Langmuir*, vol. 19, no. 24, pp. 0–4, 2003.

[71] L. Cucullo, M. Hossain, V. Puvanna, N. Marchi, and D. Janigro, “The role of shear stress in Blood-Brain Barrier endothelial physiology,” *BMC Neurosci.*, vol. 12, no. 1, p. 40, 2011.

[72] C. Hajal *et al.*, “In vitro models of molecular and nano-particle transport across the blood-brain barrier In vitro models of molecular and nano-particle transport across the blood-brain barrier,” *Biomicrofluidics*, vol. 42213, no. 12, 2018.

[73] M. B. Chen, J. A. Whisler, J. Fröse, C. Yu, Y. Shin, and R. D. Kamm, “On-chip human microvasculature assay for visualization and quantification of tumor cell extravasation dynamics,” *Nat. Protoc.*, vol. 12, no. 5, pp. 865–880, 2017.

819 **Acknowledgements**

820

821 M.C. was supported by Ermenegildo Zegna Founder's scholarship and then by the MIT-POLITO
822 grant (BIOMODE - Compagnia di San Paolo) under the joint "Doctorate of Bioengineering and
823 Medical-Surgical Sciences" of University of Turin and Politecnico di Torino. Y.S. and R.K. were
824 supported by grants from the Cure Alzheimer's Fund. T.O. was supported by research fellow overseas
825 (Japan Society for the Promotion of Science). R.K. and T.O. also acknowledge the support of National
826 Science Foundation for a Science and Technology Center on Emergent Behaviors of Integrated
827 Cellular Systems, (CBET-0939511). C.H. and R.K. were supported by the National Cancer Institute
828 (U01 CA202177). M.C., V.C., and R.K. also acknowledge the support of the research collaborations
829 and exchanges program between MIT and POLITO (MITOR project NANOCAB).

830

831 **Author contributions**

832

833 All authors designed the experiments. M.C. performed majority of experiments, analyzed all data,
834 and wrote the manuscript. Y.S. designed the microfluidic device and highly contributed to perform
835 immunocytochemistry, permeability assays and vascular parameters analysis. T.O. designed and
836 contributed to RT-PCR experiments, schematic drawings of this paper, statistical tests, discussion
837 and writing of the manuscript. C.H. and M.C. performed vascular parameters analysis. R.K. and V.C.
838 co-supervised the project. V.C. provided inputs in the writing of the manuscript. R.K. provided
839 critical inputs to the experimental design and writing of the manuscript. All authors reviewed and
840 accepted the manuscript.

841

842 **Additional information**

843

844 **Competing financial interests**

845 R.K. is co-founder and has a significant financial interest in AIM Biotech, a company that

846 manufactures microfluidic systems.